Biosensors and Bioelectronics 74 (2015) 644–651

Contents lists available at ScienceDirect

Biosensors and Bioelectronics

journal homepage: www.elsevier.com/locate/bios

Tyrosinase conjugated reduced graphene oxide based biointerface for bisphenol A sensor

K. Kamil Reza *, Md. Azahar Ali, Saurabh Srivastava, Ved Varun Agrawal, A.M. Biradar

Biomedical Instrumentation Section, National Physical Laboratory (CSIR), Dr. K.S. Krishnan Marg, New Delhi 110012, India

ARTICLE INFO

Article history:
Received 3 May 2015
Received in revised form
6 July 2015
Accepted 10 July 2015
Available online 11 July 2015

Keywords:
Reduced graphene oxide
Nanocomposite
Bisphenol A
Tyrosinase
Electrochemical sensor

ABSTRACT

We have fabricated a nanocomposite of reduced graphene oxide (rGO) sheets and chitosan (Cn) polymer based highly sensitive electrochemical biosensor for detection of bisphenol A (BPA). The two-dimensional structure and chemical functionality of rGO and Cn provide an excellent electrode surface for loading of tyrosinase enzyme molecules. This rGO–Cn nanocomposite is capable of effectively utilizing their superior conductivity, larger effective surface area and superior electrochemical performance due to its synergistic effect between rGO and Cn. The structural, morphological and electrochemical characterizations of nanocomposite sheets have been performed by electron microscopy, X-ray diffraction, FTIR and Potentiostat/Galvanostat techniques. This fabricated biosensor is sensitive to nanomolar (0.74 nM) concentration of BPA and detection time is 10 s compared to conventional BPA ELISA kit (0.3 μg/L and 2.5 h). The rGO–Cn based biosensor exhibits a higher sensitivity (83.3 $\mu A\,nM^{-1}\,cm^{-2}$), wider linearity (0.01–50 μM) with good selectivity towards BPA. This biosensor is capable to quantify real sample of BPA using packaged drinking water bottles. This rGO–Cn nanocomposite sheets emerges as a potential electrode material for detection of other estrogenic substrate.

1. Introduction

Polymer based products have potential demands in our daily life for its reusability, recycle ability and durability. Bisphenol A (BPA), 2,2-bis(4-hydroxyphenyl) propane ($C_{15}H_{16}O_2$) is utilized as recyclable polymer that commonly used in package drinking water bottles, baby bottles and food packaging industries (Vandenberg et al., 2007). This phenolic compound has similar chemical structures of natural estrogen and increased interfering effects in the endocrine system in humans causing heart diseases/obesity (Melzer et al., 2012) abnormalities in liver functions (Trasande et al., 2012), cancer (Nichols et al., 2014) etc. Further, BPA and its other phenolic compounds pose a natural threat to the environment and drinking water sources as they leaches into them easily as an environmental waste. Collectively, it has become biggest man-made threat to environment as well as human health and need an urgent efficient and selective device for routine quantification of BPA. There are several methods available for state of art tools for detection of BPA such as liquid chromatography, chemiluminescence, ELISA technique, etc. (Vandenberg et al., 2007). These commercial tools are expensive, time consuming, lack of expertize with complex procedure for volume extraction whereas electrochemical biosensor is a powerful tool for real time monitoring of analytes which provide in situ analysis, low cost, portable, rapid and widely accepted analytical system for detection of BPA (Reza et al., 2013). Furthermore, nanostructured based electrochemical biosensors show high selectivity, high stability and improved sensitivity towards the target analyte (Reza et al., 2014a).

Graphene is a two-dimensional (2D) planar structured zero bandgap carbon allotrope (Geim and Novoselov, 2007). Graphene shows unique properties like ballistic conductivity, faster heterogeneous electron transfer, larger planar surface area, high mechanical strength and ease of functionalization. These properties of graphene can be suitable for various applications in electronic devices, transparent conductors and drug diagnostics (Feng et al., 2013). Additionally, the surface properties of graphene have been customized by chemical modification to synthesize graphene oxide (GO) and reduced graphene oxide (rGO) as new generation smart materials. The presence of oxygen containing functional groups on rGO at edge and basal planes produces defects sites for good conductivity after its chemical reduction. These active sites promote faster heterogeneous electron transport (HET) along the surface with higher charge carrier mobility (Compton et al., 2011). Graphene and its oxide derivatives specially nano-composites have shown significant progress in drug delivery, nanomedicine, biosensors and bio-imaging (Yang et al., 2013). These nanocomposites possess excellent absorptivity, superior conductivity

* Corresponding author. Fax: +91 1145609152.
E-mail address: kamilreza@gmail.com (K.K. Reza).

http://dx.doi.org/10.1016/j.bios.2015.07.020
0956-5663/

and higher stability leading to an excellent electrode materials with faster carrier mobility (Georgakilas et al., 2012). The functional property of GO and rGO are widely explored for conjugation with different biomolecules including enzymes, proteins, antibodies etc. The –COOH groups in rGO are utilized for the higher loading of biomolecules due to the strong bond formation with aminated groups of polymers and enzymes (Parlak et al., 2014).

Graphene sheets based composites are being explored for the emerging new fields including bioimaging, drug delivery as the properties of composites show remarkable improvement in the aspect ratio as well as in the surface to volume ratio (Stankovich et al., 2006). The nanofiller aspect ratio, the percolation threshold and the nature of the nanofiller/matrix interface play an important role in improving the electrical, optical, thermal and mechanical properties in the newly formed graphene polymer nanocomposites through controlled interphases (Terrones et al., 2011). Researchers are currently working on surface modifications of graphene based platforms to synthesize new class of conductive nanostructured materials focuses on the following challenges: (a) generate the lowest number of defects within the graphene sheets, (b) improve the graphene compatibility with polymer matrices (good dispersion and low percolation threshold), (c) impart resistance to the chemical or electrochemical reduction, and (d) reduce the sheet-sheet junction resistivity in order to allow electronic transport (Terrones et al., 2011). The applications of carbon materials including carbon nanotube and their composites/hybrids with polymers, metals, metal oxides, etc. have extensively explored in various fields (Shearer et al., 2014). Carbon composites/hybrids offer access to both a large surface area required for gas/liquid–solid interactions and an extended interface, through which charge and energy transfer processes create synergistic effects that result in unique properties and superior performance. Synergistic effect arises between two analogous structures in size/volume fraction of the two phases enables access to a high specific surface area of the active compound as well as to a large interfacial area between the two components. These large interfacial areas are responsible for improvement in charge transfer along the surface with higher loading capacity (Shearer et al., 2014).

GO with biocompatible polymers like polyethylene glycol, chitosan (Cn) and dextran have shown promising results in biological applications (Feng et al., 2013). GO based composites are being investigated extensively in medical diagnostics for their unique stability in physiological solutions. Further, rGO composite electrode would facilitate high electron transfer between the redox-active species resulting in enhanced electrochemical response (Ali et al., 2014a). Cn is a natural biocompatible, biodegradable and high mechanical strength biopolymer having excellent film forming ability. The carboxylated groups of rGO can provide non-covalent functionalization sites for the protonated amine terminal groups of Cn polymer. The composite of rGO and Cn can act as electron donor and acceptor show significant improvement of electron transfer from electrolyte to current collector (Georgakilas et al., 2012) due to its synergistic effect. Al-Mashat et al. reported H_2 gas sensor using graphene/poly-aniline nanocomposite (Al-Mashat et al., 2010). Kotchey et al. demonstrated enzymatic oxidation using horse radish peroxidase on GO sheets for fabrication of a field effect transistor sensor (Kotchey et al., 2011). A pathogenic bacterium sensor was developed by utilizing a composite of graphene, Fe_3O_4 and Cn (NasseráAbdelhamid, 2013). A free-standing flexible rGO/nafion film has been fabricated by applying a simple solution chemistry for biosensor application (Choi et al., 2010).

We report here a highly sensitive and selective biosensor platform using tyrosinase (Tyrs) enzyme functionalized rGO and Cn nanocomposite for the determination of BPA. The nanocomposite offers active functional groups (–COOH, $–NH_2$, etc.) that gives stable surface for enzyme immobilization and the enhanced electrochemical properties reflect the activation of synergistic effect in this nanocomposite which eventually gives higher sensitivity and wider linear range. The rGO–Cn nanocomposite based electrode was fabricated using electrophoretic deposition (EPD) on indium tin oxide (ITO) glass substrate.

2. Experimental

2.1. Materials

BPA, tyrosinase (from mushroom, >1000 units mg^{-1}, pI 5.92) and all other chemicals (analytical grades) were obtained from Sigma Aldrich, USA. Phosphate buffer solution (PBS) (50 mM, pH 7.0) was used as the electrolyte in all electrochemical experiments (50 mM, pH 7.0) containing 5 mM $[Fe(CN)_6]^{3-/4-}$. Double distilled water (resistivity 18.2 MΩ was used from Millipore water purification system for all experiments.

2.2. Apparatus

High resolution-transmission electron microscope (HR-TEM, Tecnai G20-stwin), scanning electron microscopy (SEM, LEO-40) and Fourier-transform infrared (FTIR, Perkin–Elmer, Model 2000) techniques were used for characterizations of rGO–Cn based electrode and bioelectrode. The cyclic voltammetry (CV) and electrochemical impedance spectroscopy (EIS) have been conducted for electrochemical properties and response studies using Autolab, Potentiostat/Galvanostat electrochemical analyzer.

2.3. Electrophoretic deposition of rGO–Cn

The proposed mechanism for fabrication of electrode and immobilization of Tyrs on the surface of rGO–Cn is shown in Scheme 1. ITO coated glass substrate was cut into small pieces (0.5 cm × 2.0 cm) and immersed in a solution of H_2O_2:NH_3:H_2O in the ratio of 1:1:5 (*v/v*) and kept under oven for 1 h at 80 °C. Subsequently, the hydrolyzed ITO plates were washed with double distilled water and dried at 25 °C.

10 mL solution of the well-dispersed colloidal solution (in acetic acid) of rGO and Cn (mixed in ratio of 1:10) was prepared by sonication for about 30 min. The EPD technique was utilized for the fabrication of rGO–Cn electrode in a two-electrode cell containing the colloidal suspension by applying 40 V DC voltage for 180 s. Platinum foil acts as the cathode and the ITO-coated glass substrate of sheet resistance (28 Ω cm^{-1}) as the anode. The two electrodes were separated by 1 cm and placed parallel to each other, and dipped in the rGO–Cn colloidal suspension during deposition. The deposited electrode was washed with de-ionised water followed by drying.

Fresh solution of Tyrs (mg/mL) was prepared in PBS (50 mM, pH 7.0) and was uniformly spread (10 μL) on the surface of rGO–Cn. Presence of functional groups like amino and hydroxyl groups in Cn facilitates immobilization of enzymes via covalent bonding for biosensor application (Reza et al., 2014b). This polymer works as cross linker as well as binder between rGO and Tyrs enzyme. Also, the amine groups of Tyrs enzyme bind with carboxylic groups of rGO sheets by formation of covalent bond. An additional advantage of Cn polymer is the high hydrophilic nature due to the large number of hydroxyl groups present on its backbone facilitates enzyme loading (Guibal, 2005). After immobilization, the rGO–Cn/ITO bioelectrode was stored in a humid chamber for 12 h at room temperature. The bioelectrode (Tyrs/rGO–Cn/ITO) was washed thoroughly with PBS (50 mM, pH 7.0) containing 0.9% NaCl to remove any unbound enzyme and stored at 4 °C.

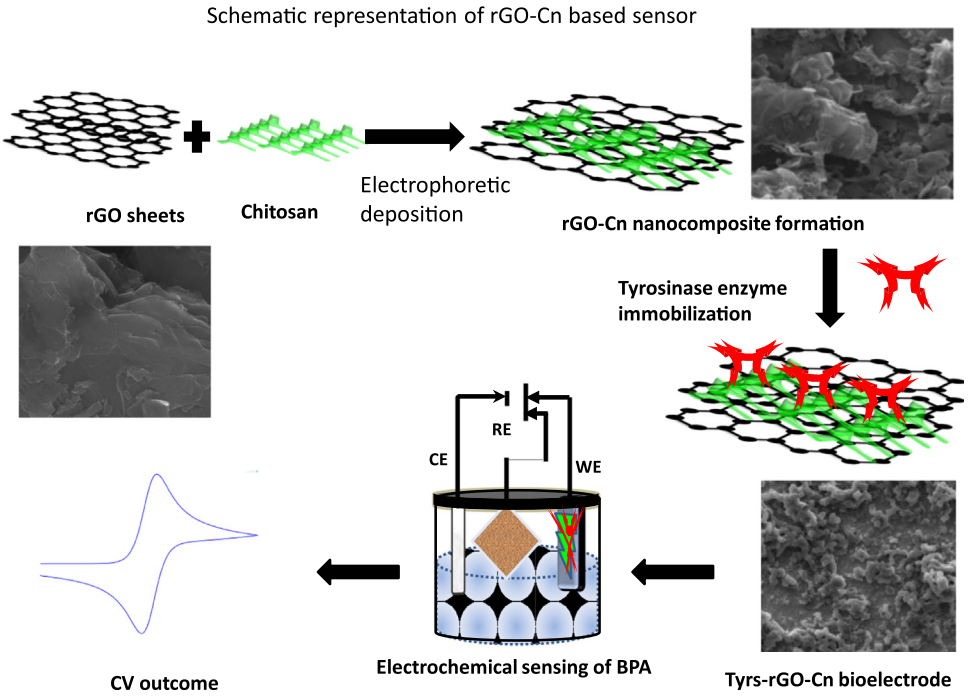

Scheme 1. : The fabrication of Tyrs–rGO–Cn/ITO electrode for BPA detection.

3. Results and discussion

3.1. Material characterization

Fig. 1 shows TEM images of rGO sheets and rGO–Cn nanocomposite. The well-suspended rGO sheets have been dispersed in acetonitrile solvent and drop casted onto a holey carbon coated copper grid for the TEM imaging. Fig. 1 shows morphology of the rGO sheets prior to Cn incorporation. The high magnification image clearly depicts the dense network of graphene sheets and some of the sheets of rGO are found to be overlapped and turned into wrapped wrinkles. Fig. 1(b) shows an image of single sheet of pristine rGO without any wrinkles. Fig. 1(c) shows a TEM image of the modified surface morphology of rGO sheets after composite formation with Cn. The nanocomposite sheets show a wrinkle free surface which may be due to bond formation between amino ($-NH_2$) groups of Cn and –COOH groups of rGO. This bonding has led to a new structure of multilayer rGO sheets due to aggregation among the layers. These nanosheets have a smooth surface and their edges are clearly visible in Fig. 1(d). This nanocomposite is composed of few layers of sheets of rGO–Cn. This amalgamation of polymer and sheet has proved to be a strong thin film formation ability which leads to a highly stable electrode formation.

The morphological structure of rGO and rGO–Cn before and after enzyme incorporation has been confirmed by SEM studies (Fig. 2(a–c)). In rGO electrode (image a), the multilayer graphene sheets are clearly visible. The graphene sheets are stacking each other forming thicker sheets due to π–π interaction between them. After incorporation Cn polymer, a morphological change is observed due to their strong interactions between –COOH groups of rGO and $-NH_2$ groups of Cn by forming amide bond (CO–NH). As a result of nanocomposite structure, aggregations of rGO sheets with polymer chain are visible (image b). In the blended system, both components are in the size range of a few microns, rGO–Cn structure appeared as a continuous network over the surface of fabricated electrode. On addition of tyrosinase on rGO–Cn surface has resulted in uniform spreading of enzyme due to the formation of amide bond. The arranged network of enzyme has wrapped the whole surface of nanocomposite, as evident from the image (c) leading to an excellent electrochemical biosensor for BPA detection. Fig. 2(d) shows the typical powder X-ray diffraction (XRD) pattern (copper K_α radiation) of the as-prepared rGO in the range of 10–70°. A characteristic broad peak is found at $2\theta = 24°$ corresponding to the interlayer spacing of 0.37 nm. This dominant peak for (002) reflection plane indicates the formation of rGO.

The interaction between rGO, Cn and tyrosinase enzyme have been confirmed by FTIR spectroscopic studies. The characteristics peaks of rGO–Cn (a) and Tyrs–rGO–Cn (b) spectra can be seen in Supplementary information (Fig. S1). The variation of characteristic peaks at 1636 cm^{-1} of –C=O stretching band of the amide groups and 1541 cm^{-1} of –N–H bending of secondary amide in rGO and rGO–Cn spectra may be due to amide bond formation between rGO and Cn (Pan et al., 2011). There is strong possibility of interaction might be due to hydrogen bonding and electrostatic interactions between polycationic chitosan molecules and negatively charged oxygen groups on rGO surface. The presence of peaks at 1643 cm^{-1} for acylamide I is due to –C=O stretching and the peak at 1537 cm^{-1} for acylamide II belongs to –N–H bending and C–N stretching of vibrational bands of amide groups of Tyrs (spectra c) (Wu et al., 2012). Moreover, the peaks at 1076 cm^{-1} and 3348 cm^{-1} in rGO spectra may be due to the –C–O–C– vibration and O–H stretching, respectively, have been shifted because of Cn and Tyrs interactions.

3.2. Electrochemical studies

CV analyses of electrodes are carried out in presence of redox species of $[Fe(CN)_6]^{3-/4-}$. The increasing order of current value in CV studies of the electrodes are Cn (0.104 mA), ITO (0.541 mA), Tyrs–rGO–Cn/ITO (0.658 mA), rGO (0.711 mA) and rGO–Cn/ITO (0.750 mA) (Fig. 3(i)). The rGO–Cn and rGO electrode show higher redox current responses compared to bare ITO electrode. The larger surface area and reduced functional groups of rGO and rGO–Cn can enhance the heterogeneous electron transfer of electrons and diffusion along the surface of the rGO sheets resulting in higher electrochemical current compared to bulk ITO electrode. The

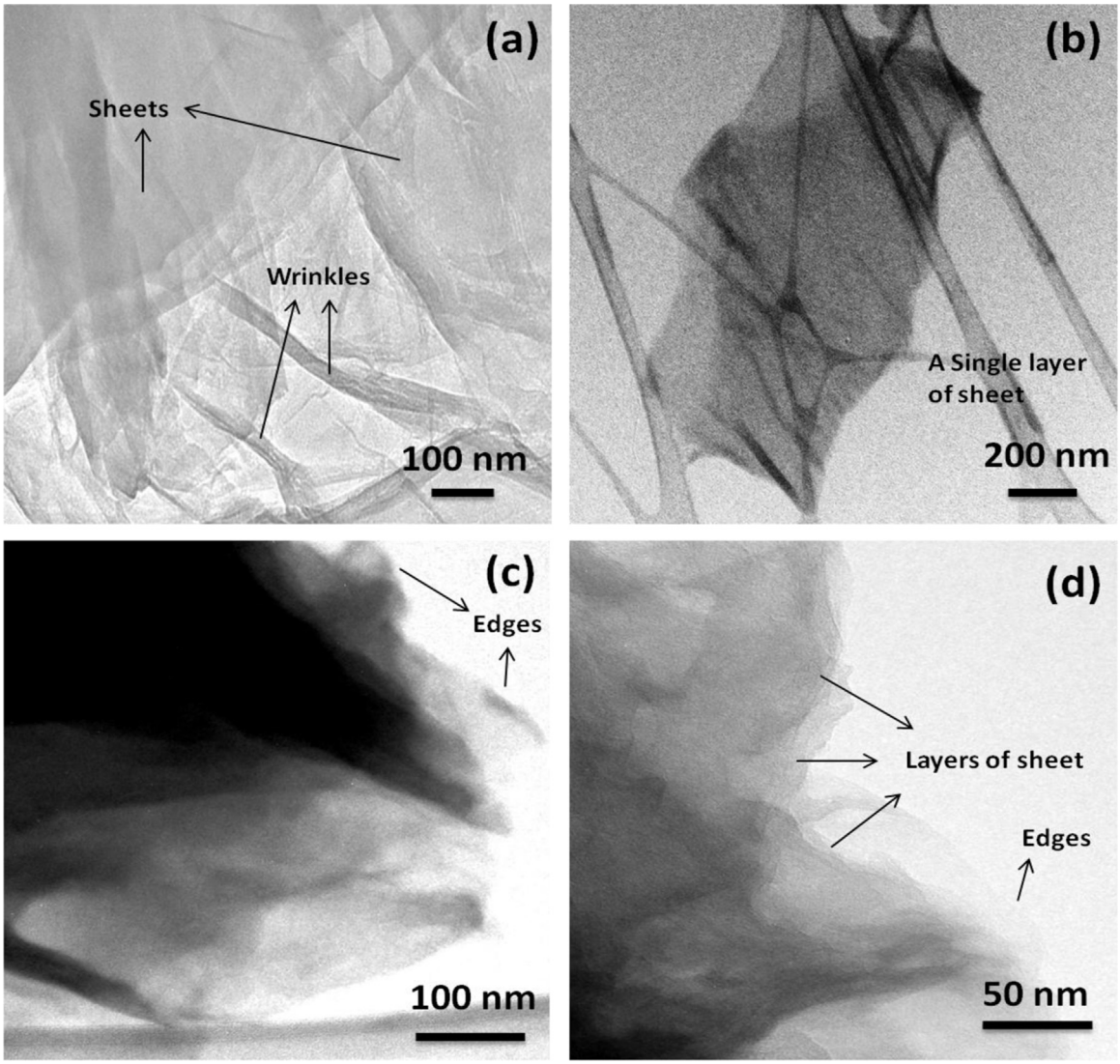

Fig. 1. (a) TEM image of rGO sheets (b) single layer sheet of rGO (c) nanostructure of rGO and Cn composite (d) high resolution nanocomposite image of rGO and Cn where layers and edges are clearly visible.

higher potential difference of rGO electrode compared to rGO–Cn electrode indicating slow electron transfer rate towards current collector. The higher amperometric response of rGO–Cn than other electrodes might be due to the synergistic effect between rGO and Cn resulting improved electrochemical behavior (Shan et al., 2010). However, immobilization of enzyme on the Tyrs–rGO–Cn/ITO electrode surface might have blocked the electron transport during electrochemical reaction causing lowering of current value. Also, the value of peak-to-peak potential separation (ΔE_p) is observed to be 0.33 V in rGO–Cn/ITO electrode while 0.39 V (ΔE_p) is observed for Tyrs–rGO–Cn/ITO electrode. This lower value of (ΔE_p) in rGO–Cn/ITO film implies better electron rate coefficient in rGO–Cn/ITO film as Tyrs modified electrode causes hindrances in the electron transfer due to attachment of biomolecules.

Further, we have conducted the scan rate studies to understand the electrochemical behavior of electrodes shown in Fig. 3(iv). The straight lines of the oxidation and reduction peak currents as a function of the square root of scan rates in the range of 10–100 mV/s shows linear increase system (Fig. 3(iv), inset). The linear relationship of peak current (I_p) versus square root of scan rate ($\upsilon^{1/2}$) in rGO films is derived from the Nernstian equation which shows interfacial activities of electro-active components in the process of adsorption and desorption (Choi et al., 2010). The redox peak potential is found to be shifted (i.e., anodic peak potential toward positive and cathodic peak potential toward negative) as the scan rate increases indicating a diffusion control process and obeys the following anodic (I_A) and cathodic (I_C) Eqs. (1) and (2) with slopes and intercepts as follows:

$$I_A(\text{bioelectrode}) = 81.3\ \mu A + 9.44 \times 10^{-5}\ (A^2 m V^{-1} s)^{1/2} \times \left[\text{Scan rate}\left(mVs^{-1}\right)\right]^{1/2};\quad r^2 = 0.997 \tag{1}$$

$$I_C(\text{bioelectrode}) = -144.50\ \mu A - 7.01 \times 10^{-5}\ (A^2 m V^{-1} s)^{1/2} \times \left[\text{Scan rate}\left(mVs^{-1}\right)\right]^{1/2};\quad r^2 = 0.997 \tag{2}$$

In Nernstian or reversible systems, the peak current is obtained by the Randles Sevcik method, described in Eq. (3)

$$I_p = 2.69 \times 10^5 n^{3/2} A D^{1/2} C \upsilon^{1/2} \tag{3}$$

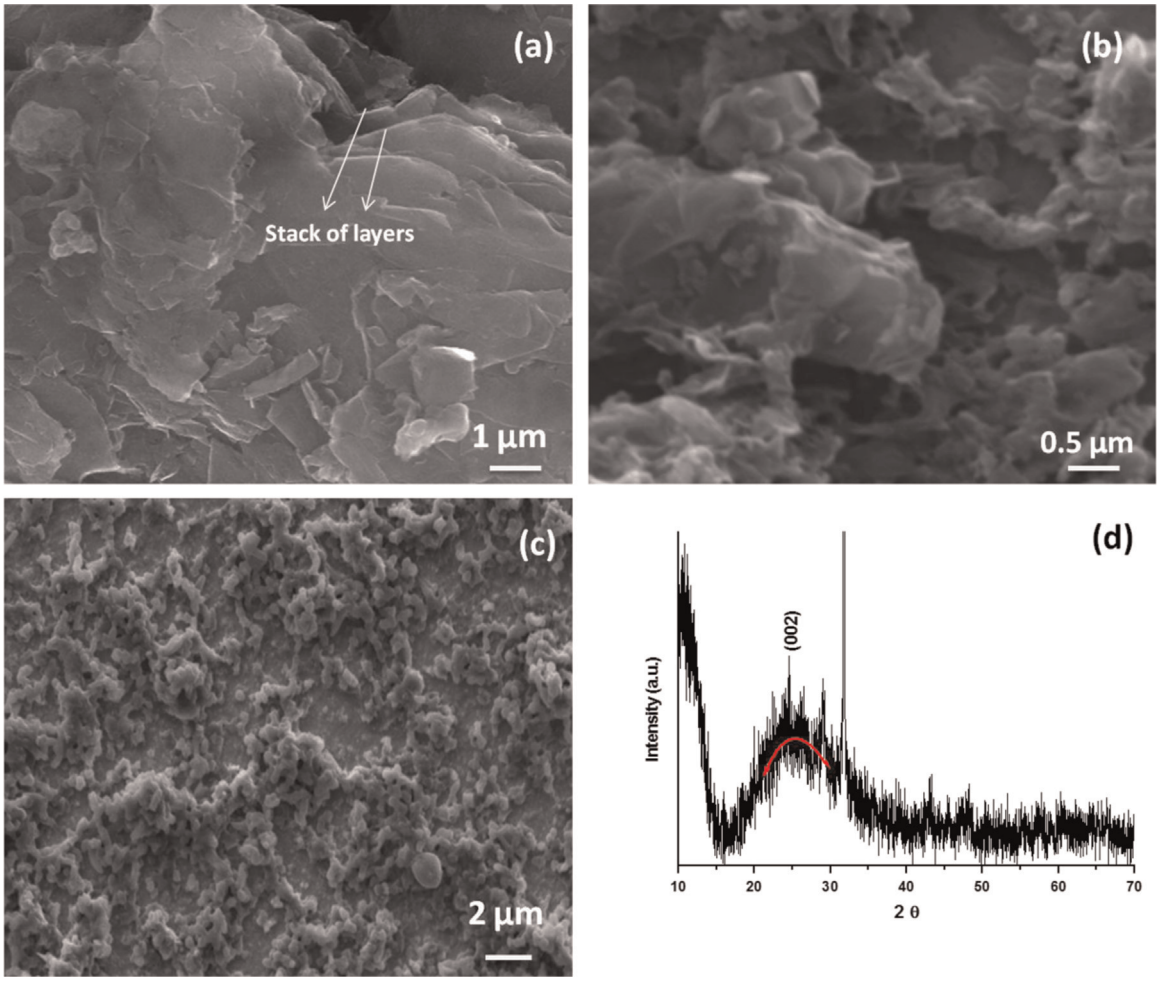

Fig. 2. (a) SEM image of rGO on ITO substrate where stack of layers are visible. (b) Nanocomposite structure of rGO and Cn polymer electrode after electrophoretic deposition (c) enzyme functionalized Tyrs–rGO–Cn/ITO bioelectrode. (d) XRD spectra of rGO.

where I_p is the peak current (0.48 mA), n is the number electrons transferred in the redox event (1), A is the area of the interface (0.25 cm^2), D is the diffusion coefficient of the transferred species, C is the concentration (5 mM) and υ is the scan rate (20 mV/s). The magnitude of diffusion coefficient has been found as 1.02×10^{-4} cm^2/s. The fabricated rGO–Cn provide a higher order value of D (1.02×10^{-4} cm^2/s) compared to other materials including CdS quantum dots (Ali et al., 2014b) (6.3×10^{-6} cm^2/s) and CNT-NiO (Ali et al., 2015) matrix (2.82×10^{-9} cm^2/s) may be due to synergistic effect of the composite material.

In EIS, the impedance is calculated by charge transfer resistance (Nyquist diameter, R_{CT}) in presence of electrolyte solution which depends on the dielectric and insulating characteristics at the electrode/electrolyte interface (Fig. 4(i)). The R_{CT} values of Tyrs–rGO–Cn/ITO (curve *a*), rGO–Cn/ITO (curve *b*) have been found as 1.83 kΩ and 400 Ω, respectively. The increased R_{CT} value of Tyrs–rGO–Cn bioelectrode over rGO–Cn electrode is perhaps due to hindrance in the electron transfer as a result of enzyme immobilization. The heterogeneous electron transfer rate (HET or κ_e) and time constant (τ) of the electrodes have been calculated by the following equations:

$$\kappa_e = RT/\left(n^2F^2AR_{CT}C\right) \quad (4)$$

and

$$\tau = R_{CT}C_{dl} \quad (5)$$

where R=universal gas constant, T=temperature, n=number of electron involved in redox reactions, A=effective area of electrode, F=Faraday constant, C=concentration of redox couple, C_{dl}=double layer capacitance. The κ_e value of rGO–Cn/ITO electrode is obtained as 4.32×10^{-5} cm/s which is larger than the bioelectrode Tyrs–rGO–Cn/ITO (1.56×10^{-5} cm/s) indicating faster electron transfer among the redox couples. The tyrosinase enzyme immobilization on the surface of rGO–Cn electrode provides hindrance to the electron transfer resulting in slower electron transfer rate constant than the rGO–Cn/ITO electrode. Further, high value of time constant (τ) for Tyrs–rGO–Cn/ITO bioelectrode (7.86 ms) shows slower diffusion rate of $[Fe(CN)_6]^{3-/4-}$ ions than rGO–Cn/ITO electrode (5.73 ms) at the solution/electrode interface. The pH value of 7.0 was chosen for all studies relating to electrochemical activity and bisphenol A biosensing as tyrosinase retain their natural structure at room temperature (25 °C).

3.3. Detection of bisphenol A

The CV responses for the fabricated bioelectrode have been investigated (Fig. 3(ii)) in presence of various BPA concentrations ranging from as small as 10 nM to a larger concentration of 50.0 µM. The gradual increase in peak current is observed with increases concentration of BPA (Fig. 3(ii)). This is attributed to the presence of Tyrs on electrode surface, which chemically converts bisphenol A into 2, 2-bis(4-phenylquinone) propane. During enzymatic reaction, the generated electrons during the oxidation of BPA are transferred to the rGO–Cn electrode through electrolyte

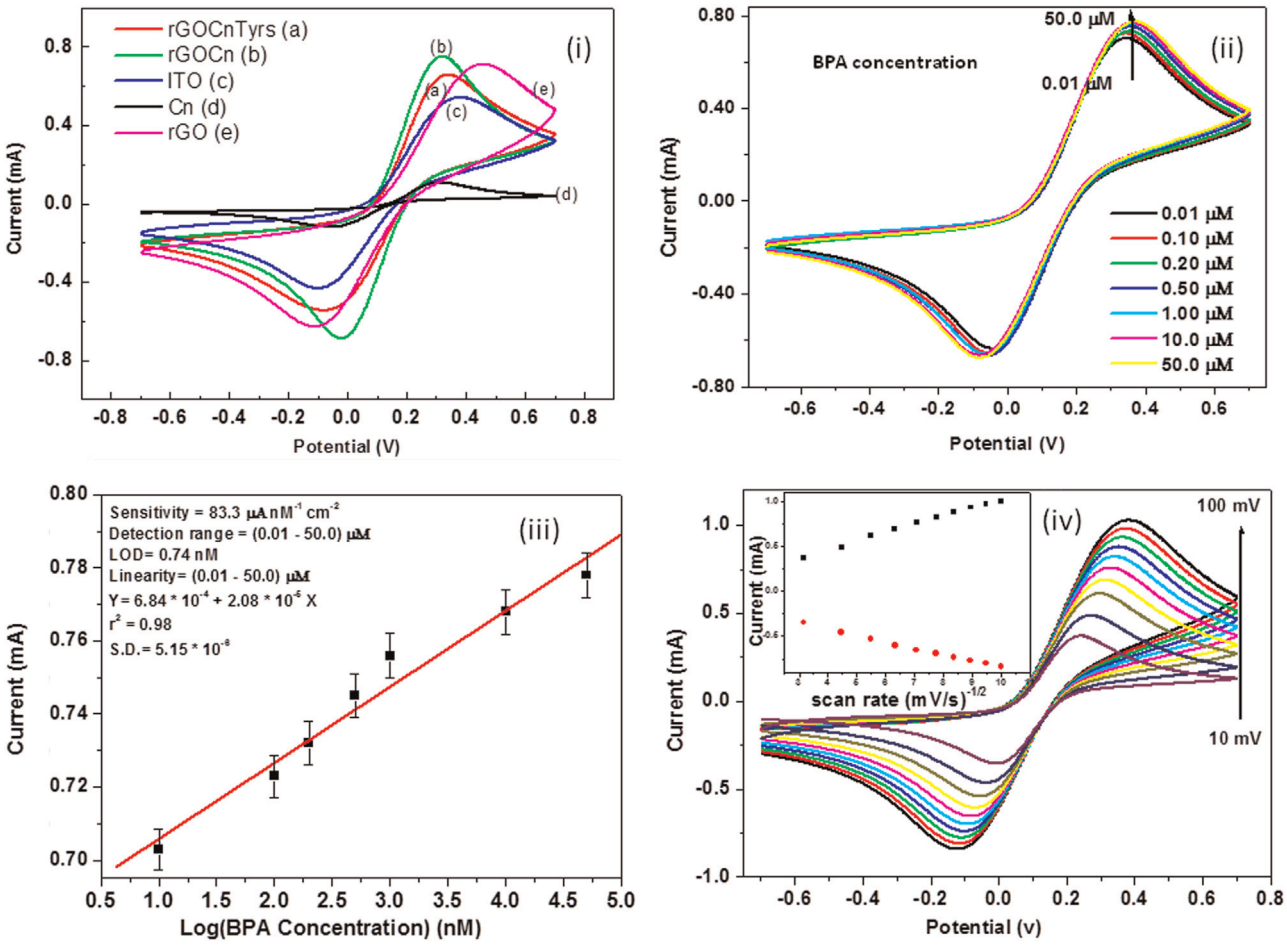

Fig. 3. (i) Cyclic voltammetry (CV) study of (a) Tyrs rGO–Cn (b) rGO–Cn and (c) ITO electrodes in the PBS containing 5 mM $[Fe(CN)_6]^{3-/4-}$. (ii) Electrochemical response curve (sensing study) of Tyrs–rGO–Cn/ITO bioelectrode as a function of BPA concentration (0.01–50 μM) in the PBS containing 5 mM $[Fe(CN)_6]^{3-/4-}$. (iii) Calibration curve between BPA concentration and the amperometric current response of the sensor (iv) CV of Tyrs–rGO–Cn/ITO bioelectrode as a function of scan rate (10–100 mV/s) and inset shows variation of current as function of square root of scan rate indicating a diffusion controlled process.

solution resulting in increased redox current. Thus, other than mediator electrons, the change in the redox current is responsible for generated electrons from enzymatic reaction. Also, the surface of rGO–Cn nanocomposite might provide larger active surface area with faster electron transfer rate due to synergistic effect through an interfacial area for better electrochemical oxidation. Further, strong and stable binding of tyrosinase enzyme with electrode have shown high enzyme loading which enhances the biosensor characteristics (Wu et al., 2012). Also, HET in rGO occurs at edges or at defects in basal plane that is responsible for larger flow of electrons between rGO and enzyme molecules. Also higher surface of area of the nanocomposite sheets provide large amount of defects that can activate the electroactive sites for higher sensing efficiency (Pumera, 2011).

A linear relationship between peak current and concentration of bisphenol A (0.01–50.0 μM) has been observed (Fig. 3(iii)). The regression equation for the sensor calibration curve is given below

$$I(\mathrm{A}) = 6.84 \times 10^{-4}\ \mathrm{A} + 2.08 \times 10^{-5}\ [\mathrm{A/nM}] \times (\mathrm{BPAConc.})\ \mathrm{nM} \quad (6)$$

Further, it shows a fast response time of 10 s in a wide range of BPA concentration (0.01–50.0 μM). The value of sensitivity (83.3 μA nM^{-1} cm^{-2}) of this fabricated biosensor is higher compared to the biosensors based on polypyridyl ruthenium electrode (0.22 μA μM^{-1}) (Li et al., 2010); thionine modified carbon paste (85.4 ± 1.5 nA μM^{-1}) (Portaccio et al., 2010); nanographene based electrode (3.10 nA nM^{-1}) (Wu et al., 2012); graphene/silk peptide based electrode (2.51 nA nM^{-1}) (Qu et al., 2013). This may be due to higher charge transfer arising from large interfacial areas that result in superior electrochemical properties of the rGO nanocomposite sheets as well as film forming ability of Cn proving better platform for sensing. This composite electrode provide wider linear range and lower detection limit (0.74 nM) for BPA than other graphene based electrodes such as nanographene (Wu et al., 2012) and Pt/graphene-CNTs (Zheng et al., 2013). The prepared biosensor (rGO–Cn) exhibits a low detection limit (0.74 nM) compared to other reported in literature (Huang et al., 2011; Portaccio et al., 2010; Zheng et al., 2013). This may be due to the larger activity at the interphases of the nanocomposite sheets and its available functional groups enhances the loading capacity of Tyrs molecules with longer stability. However, Qu et al. have reported a comparable limit of detection (0.72 nM) for BPA compared to this prepared biosensor (Qu et al., 2013). The safe upper limit of BPA in polycarbonate bottles is 22 nM (50 $\mu g L^{-1}$) which was recommended by European Food Safety Authority (EFSA) (Biedermann-Brem and Grob, 2009). Moreover, this biosensor shows a fast detection time (10 s) compared to conventional bisphenol A ELISA kit (0.3 μg/L and 2.5 h). We have summarized the sensing parameters in Table S1 (Supporting information) which shows the characteristics of this sensor along with those reported literature.

The interference study of Tyrs–rGO–Cn bioelectrode (Fig. 4(ii)) has been estimated in presence of BPA (1.0 μM) with typical

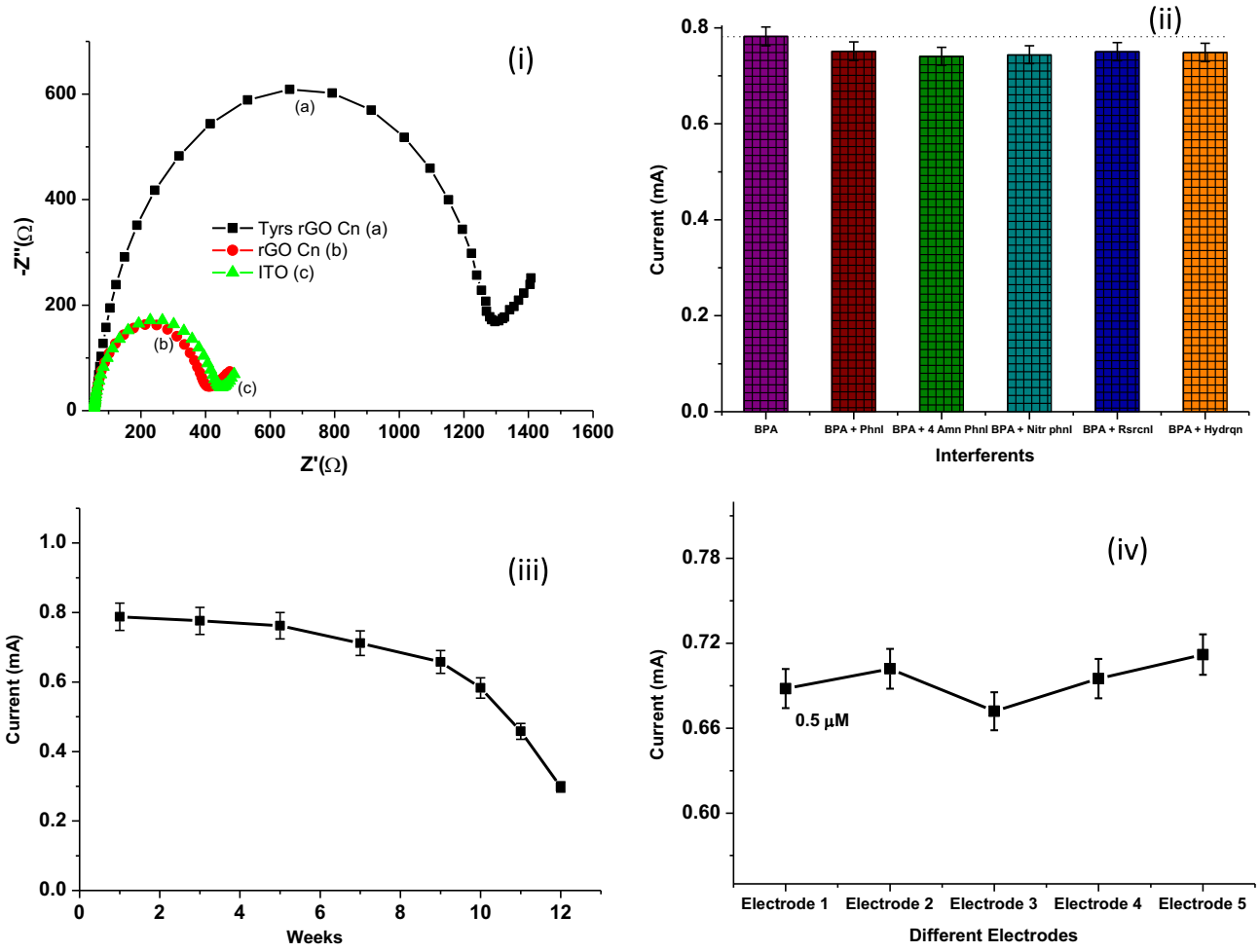

Fig. 4. (i) Electrochemical impedance spectroscopic (EIS) spectra of (a) Tyrs rGO–Cn (b) rGO–Cn and (c) ITO electrodes in the PBS containing 5 mM $[Fe(CN)_6]^{3-/4-}$. (ii) Interference study of BPA (1.0 μM) concentration with concentrations of interferents of phenol (1.0 μM), nitrophenol (1.0 μM), 4 aminophenol (0.8 mM), resorcinol (1.0 μM), and all mixers. (iii) Stability of the Tyrs–rGO–Cn/ITO bioelectrode measured as a function of weeks and current response. (iv) Reproducibility curve of five Tyrs–rGO–Cn/ITO bioelectrodes for 0.5 μM BPA concentration.

concentration of interferents such as phenol (1.0 μM), nitrophenol (1.0 μM), 4 aminophenol (0.8 mM), resorcinol (1.0 μM), and all mixers. This bioelectrode does not respond to other interferents significantly compared to BPA. However, phenolic compound make some interfering effects on the bioelectrode as BPA resembles its structures. Thus, this BPA sensitive biosensor shows an excellent selectivity with other phenolic compounds. The stability of the bioelectrode has been investigated upto 12 weeks with an interval of 2 weeks (Fig. 4(iii)). The bioelectrode remains active upto 7 weeks, losses only 10% its activity after immobilization and after that it decreases to approximately 38% of the initial response after 12 weeks. Our bioelectrode shows excellent reproducibility for BPA concentrations of 0.5 μM as evident by low relative standard deviations (RSD) (1.69%, $n=5$), proving its high-quality precision of bioelectrode (Fig. 4(iv)).

To demonstrate the practical application of this fabricated biosensor, we carried out real sample analysis of BPA using packaged drinking water bottles (Zheng et al., 2013; Singh et al., 2015). The standard addition method have been used to track the traces of BPA in three types of plastic water bottles made by polyvinyl chloride (PVC) which had been brought from local market. The sample pre-treatment step has been described in the supplementary information. A calculated amount of BPA (5.0 μM, pH 7.0) was added to each solution of the real samples which were repeated five times. The details of the BPA concentrations in three samples of PVC bottles have been depicted in Table 1. The average RSD value of the three samples were found to be 3.1% ($N=5$). The recovery values of BPA standard added with real samples were in the range of (97–104%) showing good evaluation of the fabricated sensor. The real sample study reveals the potential application of the bioelectrode as a practical tool for detection of BPA in plastic bottles.

Table 1
Determination of BPA in real samples.

Sample	Measured (μM)	Added (μM)	Calculated (μM)	Found (μM)	RSD ($N=5$) (%)	Recovery (%)
PVC 1	2.65	5.0	7.65	7.82	3.1	102.17
PVC 2	3.33	5.0	8.33	8.68	2.8	104.03
PVC 3	2.83	5.0	7.83	7.66	3.4	97.83

4. Conclusions

We have elaborated a straightforward strategy to fabricate nanocomposite sheets of rGO and Cn polymer as a smart electrode material for high performance of estrogenic biosensor. The synthesized nanocomposite sheets provide an excellent platform for loading of tyrosinase enzyme molecules by conjugating 2D

structure of rGO and excellent film forming ability of Cn. The synergistic effect of rGO–Cn nanocomposite material has shown good electrochemical characteristics for BPA monitoring. Therefore, this nanocomposite sheets shows electrochemical conductivity, larger active surface area, strong enzyme affinity and biocompatibility. As a result, rGO–Cn composite exhibits a higher sensitivity (83.3 μA/nM cm^{-2}), a wider linearity (0.01–50 μM), a low limit of detection (0.74 nM) and a longer stability with superior selectivity towards BPA. This rGO–Cn nanocomposite emerges as a potential electrode material for other target analytes.

Acknowledgment

We thank Director, National Physical Laboratory, New Delhi, India for providing the facilities. The financial support received under Department of Science and Technology projects (DST/TSG/ME/2008/18) is gratefully acknowledged.

Appendix A. Supplementary information

Supplementary data associated with this article can be found in the online version at http://dx.doi.org/10.1016/j.bios.2015.07.020.

References

Ali, M.A., Kamil Reza, K., Srivastava, S., Agrawal, V.V., John, R., Malhotra, B.D., 2014a. Langmuir 30 (14), 4192–4201.
Ali, M.A., Srivastava, S., Pandey, M.K., Agrawal, V.V., John, R., Malhotra, B.D., 2014b. Anal. Chem. 86 (3), 1710–1718.
Ali, M.A., Solanki, P.R., Srivastava, S., Singh, S., Agrawal, V.V., John, R., Malhotra, B.D., 2015. ACS Appl. Mater. Interfaces 7 (10), 5837–5846.
Al-Mashat, L., Shin, K., Kalantar-Zadeh, K., Plessis, J.D., Han, S.H., Kojima, R.W., Kaner, R.B., Li, D., Gou, X., Ippolito, S.J., 2010. J. Phys. Chem. C 114 (39), 16168–16173.
Biedermann-Brem, S., Grob, K., 2009. Eur. Food Res. Technol. 228 (5), 679–684.
Choi, B.G., Park, H., Park, T.J., Yang, M.H., Kim, J.S., Jang, S.-Y., Heo, N.S., Lee, S.Y., Kong, J., Hong, W.H., 2010. ACS Nano 4 (5), 2910–2918.
Compton, O.C., Jain, B., Dikin, D.A., Abouimrane, A., Amine, K., Nguyen, S.T., 2011. ACS Nano 5 (6), 4380–4391.
Feng, L., Wu, L., Qu, X., 2013. Adv. Mater. 25 (2), 168–186.
Geim, A.K., Novoselov, K.S., 2007. Nat. Mater. 6 (3), 183–191.
Georgakilas, V., Otyepka, M., Bourlinos, A.B., Chandra, V., Kim, N., Kemp, K.C., Hobza, P., Zboril, R., Kim, K.S., 2012. Chem. Rev. 112 (11), 6156–6214.
Guibal, E., 2005. Prog. Polym. Sci. 30 (1), 71–109.
Huang, J., Zhang, X., Liu, S., Lin, Q., He, X., Xing, X., Lian, W., 2011. J. Appl. Electrochem. 41 (11), 1323–1328.
Kotchey, G.P., Allen, B.L., Vedala, H., Yanamala, N., Kapralov, A.A., Tyurina, Y.Y., Klein-Seetharaman, J., Kagan, V.E., Star, A., 2011. ACS Nano 5 (3), 2098–2108.
Li, Q., Li, H., Du, G.-F., Xu, Z.-H., 2010. J. Hazard. Mater. 180 (1), 703–709.
Melzer, D., Osborne, N.J., Henley, W.E., Cipelli, R., Young, A., Money, C., McCormack, P., Luben, R., Khaw, K.-T., Wareham, N.J., 2012. Circulation 125 (12), 1482–1490.
NasseráAbdelhamid, H., 2013. J. Mater. Chem. B 1 (32), 3950–3961.
Nichols, C., Ding, X., Miranda-Carboni, G., Krum, S.A., 2014. Cancer Res. 74 (19 Suppl), 3192.
Pan, Y., Bao, H., Li, L., 2011. ACS Appl. Mater. Interfaces 3 (12), 4819–4830.
Parlak, O., Turner, A.P., Tiwari, A., 2014. Adv. Mater. 26 (3), 482–486.
Portaccio, M., Di Tuoro, D., Arduini, F., Lepore, M., Mita, D., Diano, N., Mita, L., Moscone, D., 2010. Biosens. Bioelectron. 25 (9), 2003–2008.
Pumera, M., 2011. Mater. Today 14 (7), 308–315.
Qu, Y., Ma, M., Wang, Z., Zhan, G., Li, B., Wang, X., Fang, H., Zhang, H., Li, C., 2013. Biosens. Bioelectron. 44, 85–88.
Reza, K.K., Srivastava, S., Yadav, S.K., Biradar, A.M., 2014a. Mater. Lett. 126, 126–130.
Reza, K.K., Singh, N., Yadav, S.K., Singh, M.K., Biradar, A., 2014b. Biosens. Bioelectron. 62, 47–51.
Reza, K.K., Singh, M.K., Yadav, S.K., Singh, J., Agrawal, V.V., Malhotra, B.D., 2013. Sens. Actuator B Chem. 177, 627–633.
Shan, C., Yang, H., Han, D., Zhang, Q., Ivaska, A., Niu, L., 2010. Biosens. Bioelectron. 25 (5), 1070–1074.
Shearer, C.J., Cherevan, A., Eder, D., 2014. Adv. Mater. 26 (15), 2295–2318.
Singh, N., Reza, K.K., Ali, M.A., Agrawal, V.V., Biradar, A.M., 2015. Biosens. Bioelectron. *68*, 633–641.
Stankovich, S., Dikin, D.A., Dommett, G.H., Kohlhaas, K.M., Zimney, E.J., Stach, E.A., Piner, R.D., Nguyen, S.T., Ruoff, R.S., 2006. Nature 442 (7100), 282–286.
Terrones, M., Martín, O., González, M., Pozuelo, J., Serrano, B., Cabanelas, J.C., Vega-Díaz, S.M., Baselga, J., 2011. Adv. Mater. 23 (44), 5302–5310.
Trasande, L., Attina, T.M., Blustein, J., 2012. Jama 308 (11), 1113–1121.
Vandenberg, L.N., Hauser, R., Marcus, M., Olea, N., Welshons, W.V., 2007. Reprod. Toxicol. 24 (2), 139–177.
Wu, L., Deng, D., Jin, J., Lu, X., Chen, J., 2012. Biosens. Bioelectron. 35 (1), 193–199.
Yang, Y., Asiri, A.M., Tang, Z., Du, D., Lin, Y., 2013. Mater. Today 16 (10), 365–373.
Zheng, Z., Du, Y., Wang, Z., Feng, Q., Wang, C., 2013. Analyst 138 (2), 693–701.